JOURNAL OF PROPULSION AND POWER
Vol. 34, No. 5, September–October 2018

Ion Heating Measurements on the Centerline of a High-Current Hollow Cathode Plume

Christopher A. Dodson*
University of California, Los Angeles, California
Daniel Perez-Grande†
Charles III University of Madrid, Leganés, Spain
Benjamin A. Jorns‡
University of Michigan, Ann Arbor, Michigan
Dan M. Goebel§
Jet Propulsion Laboratory, California Institute of Technology, Pasadena, California
and
Richard E. Wirz¶
University of California, Los Angeles, California

DOI: 10.2514/1.B36788

An experimental investigation into the correlation between ion acoustic turbulence (IAT) and anomalous ion heating in the plume of a 100 A-class LaB_6 hollow cathode is presented. Laser-induced fluorescence is employed to measure the ion velocity distribution function, and a translating ion saturation probe is used to quantify the spatial dependence of the IAT wave energy. It is found that over a range of flow rates and operating currents both the ion temperature and IAT energy increase downstream of the cathode in qualitatively similar ways. Both parameters also are shown to be impacted by operating conditions: the IAT energy and ion temperature decrease at higher flow rates and lower discharge currents. It is shown that the ratio between ion temperature and wave energy is related by a scaling parameter that depends on the background plasma parameters, and this relation is examined in the context of previous analytical work on IAT-induced ion heating.

Nomenclature

A	=	area, m^2
c	=	speed of light, m/s
c_s	=	ion acoustic speed, m/s
f	=	laser frequency, Hz
f_s	=	velocity distribution function
I	=	current, A
k	=	wavenumber, 1/m
m	=	mass, kg
n_s	=	density, 1/m^3
q	=	fundamental charge, C
T_s	=	temperature, eV
V	=	voltage, V
V_s	=	drift velocity, m/s
v	=	velocity, m/s
W	=	wave energy density, J/m^3
z	=	axial distance into the plume, m
γ	=	wave growth rate, J/m
ϕ	=	potential, V
ν	=	wave frequency, Hz
ω	=	angular frequency, rad/s
σ	=	collision cross section, m^2

Presented as Paper 2016-4838 at the 52nd AIAA/SAE/ASEE Joint Propulsion Conference, Salt Lake City, UT, 25–27 July 2016; received 4 June 2017; revision received 27 February 2018; accepted for publication 1 March 2018; published online 28 June 2018.

*Ph.D. Candidate, Aerospace Engineering; cdodson@ucla.edu. Student Member AIAA.
†Ph.D. Candidate, Aerospace Engineering.
‡Assistant Professor, Department of Aerospace Engineering. Senior Member AIAA.
§Senior Research Scientist, Thermal and Propulsion Engineering Section. Fellow AIAA.
¶Associate Professor, Mechanical and Aerospace Engineering. Associate Fellow AIAA.

I. Introduction

MANY long-duration space missions (up to 50 kh) have been proposed over the past two decades that would use electric propulsion in the form of ion [1] and Hall thrusters [2]. Hollow cathodes, which both ionize the propellant and neutralize the exhaust in most forms of electric propulsion, must also be able to meet these increasingly demanding requirements on lifetime and current. One possible failure mode for hollow cathodes for such missions is erosion caused by energetic ion bombardment, the mechanism of which has not yet been bounded or fully understood. The term "energetic" here refers to energies in excess of that explained by classical processes such as electrostatic acceleration or plasma gradients.

The initial observations of erosion of surfaces exposed to high current hollow cathode plumes were in 1988 by Rawlin [3] and Brophy and Garner [4], who saw evidence of energetic ions in both axial and radial directions. Since that time many researchers have measured the ion energy distribution function (IEDF) in hollow cathode plumes [5–9] using retarding potential analyzers (RPAs). Many of the studies show energies well in excess of the discharge voltage, which is typically 15–20 V. Although several explanations for the source of energetic ion production have been proposed, several studies suggest that ion acoustic turbulence (IAT) may be a significant contributor. Mikellides et al. [10] claimed that IAT could exist in the cathode plume, caused by a high electron Mach number and electron-to-ion temperature ratio. Experimental work by Jorns et al. [11–13] confirmed the existence of IAT in the plume, showed that the ion energy and temperature trends measured in the far plume correlated with the wave energy measurements obtained in the near plume, and found the IAT wave energy to increase with discharge current and decreasing flow rate. Theoretical work by Jorns et al. [9,14] showed qualitative agreement with a 1D kinetic model estimating ion heating on the cathode centerline, and found the measured wave energy to be sufficient to cause the formation of a hot ion tail. Additionally, measurements by Ho et al. of the keeper face of a 100 A LaB_6 cathode show that erosion rates are higher than can be explained by ions falling through the sheath potential alone, and that anomalous erosion rates correlated with operating conditions known to result in anomalously energetic ions [15].

This body of analytical and experimental work suggests that the onset of anomalous ion heating is related to the onset of IAT, and that ion heating measured locally with laser-induced fluorescence (LIF) should correlate with wave energy measurements. However, to date there has not been a direct experimental correlation locally in the plasma between the IAT energy and ion temperature. Although LIF has been performed on hollow cathode plumes (see Refs. [16,17]), the plume conditions were different from that studied here and were not focused on regimes associated with strongly developed IAT. The goal of this investigation is to examine the correlation between IAT wave energy and ion temperature using LIF and ion saturation probe techniques in the plume of a 100 A class hollow cathode. In the first section, we briefly outline the theory of IAT in the plume. In the second section, we describe the experimental setup used to measure the IAT wave energy and ion heating on the plume centerline. The third section presents experimental data analysis and results. In the fourth and final section we discuss the results and compare to a theoretically predicted scaling between IAT wave energy and ion temperature.

II. Theory

Ion acoustic waves are produced when the velocity of the electrons in the reference frame of the ions exceeds the ion acoustic speed [18], $c_s = \sqrt{(T_e + \gamma_i T_i)/m_i}$, where T_e and T_i are the electron and ion temperature in eV, m_i is ion mass, γ_i is the ratio of specific heats for ions (assumed to be equal to 3 for longitudinal compressions), the electrons are assumed to be isothermal, and it is assumed that Landau damping from ions is small. These waves can become unstable over a broad range of frequencies (typically 100 kHz to several MHz) and develop into IAT. The source of free energy in IAT is the relative drift velocity of the electrons, which transfers energy to the wave through inverse electron Landau damping. Scattering of the electrons on the waves results in what is referred to as anomalous resistivity, which can greatly exceed the classical resistivity caused by Coulomb collisions only, and Joule heating of the electron population. The ions interact with the waves through ion Landau damping, which extracts energy from the waves and heats the ions. The turbulent waves exist as a cone-shaped distribution of wave vectors whose axis is aligned with the direction of the relative electron drift velocity [18]. Along this direction the growth rate is maximum, allowing us to ignore the oblique wave components.

The dispersion relation for ion acoustic waves for the experiment considered here is given in Ref. [12], the real part of which is given by:

$$\omega_R = k(c_s + V_i) \tag{1}$$

where ω is wave frequency and k is wavenumber. It is assumed that the wavelength is long compared with the Debye length and that the plasma is uniform locally (i.e., it varies slowly compared with the wavelength of the wave). Expressing the imaginary part in terms of wave growth rate, γ, the result is [12]:

$$\gamma = 2\omega_I = c_s k\left[\left(\frac{\pi}{2}\right)^{1/2}\left(\frac{V_e' - c_s}{v_e}\right) - \left(\frac{\pi}{2}\right)^{1/2}\left(\frac{T_e}{T_i}\right)^{3/2} e^{-T_e/2T_i}\right] - \nu_i \tag{2}$$

where V_e' is the drift velocity of the electrons relative to the ions ($V_e' = V_e - V_i$), v_e is the electron thermal velocity, and ν_i is the ion collision frequency. The terms represent inverse electron Landau damping, ion Landau damping, and collisional damping, respectively. In the hollow cathode plume collisional damping is dominated by ion-neutral collisions.

As summarized in Ref. [14], there are several studies that have suggested a relationship between ion heating and ion acoustic turbulence. For the plasma environment created by a hollow cathode plume, Jorns et al. proposed a relationship based on a quasilinear formulation between the ion temperature and the wave energy [9,14], briefly described here. Ignoring nonlinear wave-wave and wave-particle-wave interactions, and assuming that the plasma is both weakly turbulent and has random phase (both of which have been verified experimentally [12]), the effect of IAT on the ion distribution function can be expressed as a diffusion operator in velocity space using quasilinear theory. This diffusion operator consists of a resonant component, which accounts for energy transfer to ions moving at the phase velocity of the wave ($v = \omega/k$), and a nonresonant component, which accounts for the superposition of waves of random phases causing periodic variations in the distribution function, the net effect of which is a broadening of the distribution function. This fluid treatment of IAT-driven ion heating neglects the resonant wave-particle interaction, assuming it to be small relative to the nonresonant component.

In the reference frame of the ions, the energy density associated the ion motion, $W_{\text{part}} = n_0 T_i$, can be related to the electrostatic energy density of the wave, $W_T = n_0 E_T$, by a scaling parameter, $\Gamma = W_{\text{part}}/W_T$, where n_0 is the zero-order plasma density (assuming quasi-neutrality) and E_T is the total energy per unit charge from the spectrum of electric field fluctuations. Note that here we are only considering the energy associated with the IAT portion of the fluctuation spectrum. The energy in the low-frequency oscillations is not considered here, but may also contribute to ion energy. The relationship between the change in ion temperature as a function of wave energy change is then given by:

$$\Delta T_i \approx \Gamma \Delta E_T \tag{3}$$

Using the dispersion relation of ion acoustic waves subject to the simplifying assumptions above yields the following expression for the energy of electrostatic waves [19]:

$$E_T = \sum_k \frac{q^2 \tilde{\phi}_k^2}{T_e(1 + 3T_i/T_e)}\left[1 + \frac{V_i}{c_s}\right] \tag{4}$$

where $\tilde{\phi}_k$ is the amplitude of the fluctuating plasma potential of acoustic mode with wavenumber k and q is the fundamental charge. This expression shows that the thermalized energy of the distribution can be related to the total wave energy.

III. Experimental Setup

A. Facility and Cathode Assembly

The experiments were performed in a 2.6 m × 5.2 m long vacuum chamber at the Jet Propulsion Laboratory, California Institute of Technology. Pumping was provided by a combination of LN_2 shrouds and cryogenic pumps, with a total xenon pumping speed of ~40 kL/s and a base pressure of ~10^{-7} Torr. Convection and ionization gauges provided pressure information. The cathode discharge was powered by a Sorensen power supply capable up to 330 A. Cathode flow control was provided by an 0–50 sccm Apex flow controller. A needle valve on a bypass leg allowed for increasing the background pressure. Research-grade xenon gas was used for all testing.

The experiments discussed in this paper were performed using a 100 A class LaB_6 hollow cathode, shown in Fig. 1a. The cathode and keeper were made of graphite and the cathode orifice plate was made of tungsten. A 100-mm-diam, 300-mm-long copper anode was located 30 mm downstream of the keeper face and concentrically aligned with the cathode. The high-power capability of the cathode required water cooling through a copper tube brazed to the anode. Tungsten sheets lined the inside of the anode to reduce the rate of sputtering from the anode to the cathode, because the sputter yield for copper is higher than tungsten. No magnetic field was applied in this test series to simplify the comparison of theory to experiment.

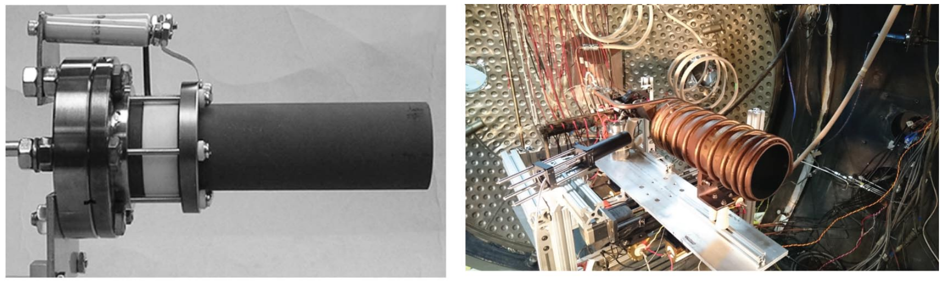

a) 100 A, 1/2" LaB_6 Hollow Cathode　　b) Cathode assembly and test configuration

Fig. 1 Cathode assembly.

Modeling by Lopez-Ortega [20] showed the maximum field to be 50 G in the region between the cathode and keeper, and to decrease with distance downstream, so magnetic field effects are neglected in this study.

The cathode assembly was mounted to two orthogonal stages that provide axial and lateral translation of the assembly, while probe and optical diagnostics remained fixed. The entire setup was mounted at the end of the vacuum chamber with the anode approximately at the chamber centerline, as shown in Fig. 1b. The anode was biased with respect to the cathode via the copper tubing, which are isolated from the chamber through a nonconducting sleeve. The cathode was kept at ground potential, with both the keeper and anode floating relative to the cathode.

B. Laser-Induced Fluorescence Diagnostic

LIF was used to measure the IVDF in the near field. The LIF technique involves measuring the Doppler shift of an absorption line of singly ionized xenon to provide the ion velocity distribution, using the relationship $v_i = c\Delta f/f_0$, where v_i is ion velocity, Δf is the difference between the laser frequency and the frequency of the absorption transition in the rest frame of the ions, f_0, and c is the speed of light. Because of its high transition probability and accessibility using diode lasers, the XeII $5d^2F_{7/2} \rightarrow 6d_2^{5/2}$ transition is excited using 834.953 nm (vacuum), resulting in fluorescence at 542.066 nm (vacuum) [21,22]. LIF is preferable to an RPA because it does not perturb the plasma, measures only a single species at a time, has a high spatial resolution, and does not require knowledge of the plasma potential (which is required for RPA measurements [see Sec. III.C.1]). A schematic of the laser optics table is shown in Fig. 2a. The laser is a continuous-wave TLB-6700 Velocity diode seed laser coupled into a TA-7616 tapered amplifier, both by New Focus. The maximum power from the tapered amplifier was 550 mW. Wavelength measurement was provided by a High Finesse WS7 wavelength meter with 60 MHz ($\pm$0.12 pm) resolution. The injection beam was modulated at 3 kHz using an optical chopper and coupled to a 50 μm optical fiber.

Inside the chamber a 62.5 μm fiber was coupled to 25 mm injection optics that provided a 2 mm spot size at a 1 m working distance, with a maximum average power of 120 mW. Figure 2b shows the optical configuration at the cathode assembly. The collection optics consisted of two 25-mm-diam lenses with 75–125 mm focal lengths. The upstream-facing lens was used to observe from the keeper face to 15 mm downstream, whereas the downstream-facing lens provided access from 15 to 60 mm downstream. The spot sizes were 0.6–1.2 mm. The collected light was focused to a 600 μm fiber connected to a Hamamatsu H10721-01 photomultiplier tube (PMT) using a bandpass filter centered at 543 nm with 11 nm FWHM acceptance. Current output from the PMT was directed to a Keithley Model 427 current amplifier, which output voltage to a Stanford Research Systems SR830 lock-in amplifier. The optical chopper was also connected to the SR830, which output the phase-sensitive detection amplified PMT signal to a National Instruments DAQ card.

Most of the LIF signals showed two peaks, referred to here as the "slow" and "fast" ion populations, with the slow population drift nearly zero. We therefore employ a dual Gaussian curve fit:

$$f_i(v) = n_{01}\sqrt{\frac{m_i}{2\pi T_{i1}}}e^{-m_i(v-V_{i1})^2/2T_{i1}} + n_{02}\sqrt{\frac{m_i}{2\pi T_{i2}}}e^{-m_i(v-V_{i2})^2/2T_{i2}} \tag{5}$$

where n_{01} and n_{02} are the densities of the two ion populations of the slow and fast populations, respectively, and V_{i1} and V_{i2} are the most probable velocities. In the following, the reported ion temperatures and mean drifting velocity stem from this deconvolution technique, an example of which is shown in Fig. 3. Hyperfine broadening was found by Huang et al. [23] and Pawelec et al. [24] to be ~450 MHz, and Stark broadening due to charged particle collisions for the densities measured are estimated by Huang (extrapolating from data presented by Manola and Konjevic [25]) to be ~20 MHz [26]. Because of the relatively large full-width half-max (FWHM) of the signal, both hyperfine and Stark broadening are therefore neglected. The primary uncertainties in the derived ion properties are then due to the deconvolution procedure and estimates of the degree of saturation broadening.

Saturation broadening occurred due to the high laser intensity (~76 mW/mm^2, assuming a top-hat spatial profile) used to maximize the signal-to-noise ratio. The amount of broadening was estimated using the approach by Chaplin et al. [27] and Smith [28] for a two-level model of this transition, and will only be briefly described here. A lineshape that consists of both Doppler broadening (a Gaussian) and natural broadening (a Lorentzian) associated with

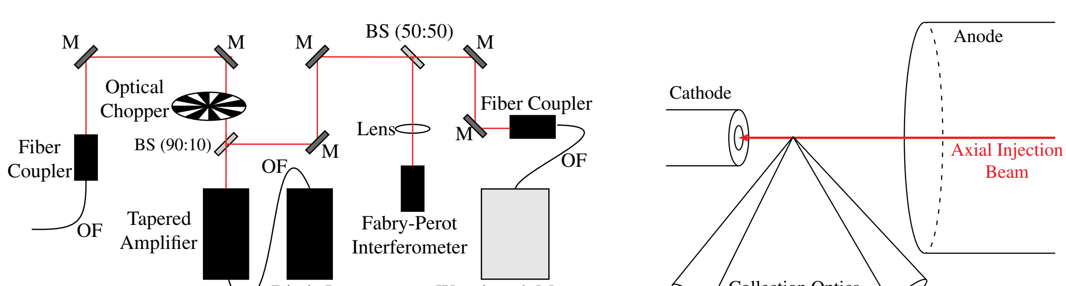

a) Optical bench (M: mirror, BS: beam splitter, OF: optical fiber)　b) Chamber configuration

Fig. 2 Laser-induced fluorescence system.

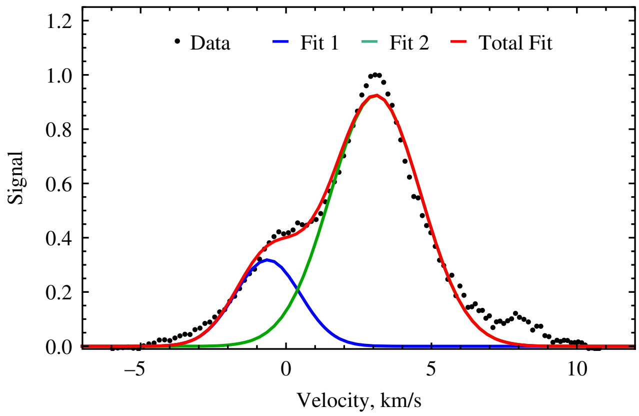

Fig. 3 Curve fits applied to the 70 A, 10 sccm IVDF at $z = 12$ mm. Fit 1 refers to the nondrifting population and Fit 2 to the drifting population. Total Fit is the double Gaussian curve fit. The raw data have had a 9-point boxcar average applied.

saturation broadening will be a Voigt profile whose FWHM is effectively the same as a Gaussian for large ratios of Doppler to natural broadening. For each LIF measurement the original Doppler broadening was iterated upon until the total FWHM of the final Voigt matched the FWHM of the fast population from Eq. (5), and the difference used to estimate the effect of saturation broadening in terms of T_i. A formal procedure in which the raw LIF measurement is deconvolved using the Doppler and Lorentzian functions before the dual Gaussian curve fitting would be more rigorous, but in order for this more complicated analysis to be justified the exact degree of saturation broadening should be known (which is not the case for these conditions). Also, other aspects of the transition, such as electron-induced excitation and quenching, would need to be incorporated into a higher-order energy level model due to the high densities in the near plume. Because of these unknowns, we therefore estimate the total uncertainty as the root-mean-square of the uncertainties due to saturation broadening and curve fitting.

C. Probe Diagnostics

Plasma probes were used to measure the properties needed to determine the turbulent wave energy in the plasma. A Langmuir probe was used for obtaining plasma density and electron temperature. An RPA was used to measure the ion energy in the far plume for comparison with near-plume measurements of ion energy obtained from LIF. This section briefly describes the operation of each as well as assumptions made in the data analysis.

1. Retarding Potential Analyzer

A four-grid-type RPA was located on the cathode centerline 350 mm downstream of the keeper face, approximately at the end of the anode, facing the cathode keeper face. The first grid of the RPA was allowed to float; the second, electron-repelling grid was biased to −10 V with respect to ground; the third grid had a variable bias voltage applied to discriminate ion energies; the fourth grid was grounded through a Keithly 427 high-impedance current amplifier. The output voltage from the amplifier provided a signal proportional to ion current to the collector with energies greater than the discriminator bias voltage. Because it is not possible to discern between singly and multiply charged ions, it was assumed that singly charged ions dominated the plasma at the RPA location. The discriminator voltage was provided by a DC power supply swept at 1 V increments from 0 to 100 V and measuring the time-averaged voltage at each step. From Ref. [29], Chap. 3, the collector current is determined as follows:

$$I_c(V_{\text{bias}}) = \frac{q^2 n_i A}{m_i} \int_{eV_{\text{bias}}}^{\infty} f_{i,c}(E - e\phi_{\text{pl}})\,\mathrm{d}E \tag{6}$$

where I_c is the collector current, V_{bias} is the discriminator bias, n_i is ion density, A is collector area, and $f_{i,c}(E)$ is the IEDF at the collector, and ϕ_{pl} is the local plasma potential. Accounting for the local plasma potential is necessary due to energy gained by the ions falling through the sheath to the collector. The value for ϕ_{pl} at the location of the RPA was not measured in these experiments, and so it was approximated to be equal to the discharge voltage, V_d. Differentiating Eq. (6), we get:

$$-\frac{dI}{dV_{db}} = \frac{q^2 n_i A_c}{m_i} f_{i,c}(E - e\phi_{\text{pl}}) \propto f_{i,c}(E - e\phi_{\text{pl}}) \tag{7}$$

where the constants were ignored because we are seeking the IEDF shape function. These differentiated data were boxcar-averaged and then normalized to the signal maximum for each measurement condition. Because it is possible that $\phi_{\text{pl}} < V_d$, the energies calculated could be slightly higher than calculated here.

2. Langmuir Probe

A cylindrical Langmuir probe was used to measure plasma density, electron temperature, and wave energy. The probe consisted of a 2-mm-long, 0.5-mm-diam cylindrical tungsten rod protruding from an alumina tube mounted vertically and fixed in location relative to the cathode assembly stage. Probe measurements were taken from 4 mm downstream of the keeper face to 3 mm upstream of the anode.

To obtain electron temperature the probe bias was swept from −70 V to +10 V relative to ground using a Kepco bipolar operational power supply. The sweep signal was provided by a Wavetek 178 waveform synthesizer swept at 30 Hz, isolated from the Kepco supply with an operational amplifier. Current was measured through a 50 Ω resistor by an oscilloscope, averaging the trace over 50 sweeps. The +10 V maximum bias voltage was chosen to avoid excessive electron current (caused by densities exceeding 10^{19} m^{-3}) that could make the probe emissive at that sweep rate. The electron temperature was inferred from an exponential fit to the probe current-voltage (IV) trace [30]. The ion current was approximated using a linear fit to the IV curve in the voltage range of approximately −40 V to −10 V. Uncertainty was approximated by applying linear regression to both the linear ion saturation and exponential electron temperature portions. Because data were only taken over the low voltage portion of the characteristic curve, it was not possible to obtain measurements of plasma potential.

To estimate the wave energy in Eq. (4) it is necessary to measure the fluctuating plasma potential amplitude spectrum in the range of frequencies associated with the IAT mode. The approach used here involves making measurements of the ion saturation current and relating this to the plasma potential fluctuation [11] using a linear perturbation analysis of the ion and electron fluid equations to obtain:

$$\tilde{\phi} \approx \frac{T_e}{q}\frac{\tilde{n}_i}{\bar{n}_i} \approx \frac{T_e}{q}\frac{\tilde{I}_{\text{sat}}}{\bar{I}_{\text{sat}}} \tag{8}$$

where $\tilde{n}_i$ is the fluctuating ion density and n_i is the time-averaged ion density, and we have assumed that the fluctuating pressure term is dominated by density fluctuations and that electron temperature fluctuations are negligible. Also implicit in this derivation is that the $\tilde{\phi} \ll \phi$, which is true for IAT that typically has $\tilde{\phi} \leq 0.01 V_d$. The probed was biased to a fixed value of −27 V, supplied by batteries to avoid any low-impedance paths to ground that could exist in a power supply. The high-speed measurements of the voltage drop across a 50Ω resistor were taken with an oscilloscope. Fourier analysis was performed in LabVIEW, which output the power spectrum up to 3.25 MHz along with the time-averaged DC voltage drop.

Steady-state values of ion saturation current in this circuit configuration were used to approximate the plasma density. Using the commonly used assumption of stationary, isotropic, cold ions, and the thin-sheath approximation [30], we have the following relationship:

$$n = \frac{I_{\text{sat}}}{e^{-1/2} q A v_{\text{sh}}} \tag{9}$$

where the ratio of density at the sheath boundary to bulk plasma, n_{sh}/n_0, is $\approx e^{-1/2}$, A is the sheath area (approximately equal to the collection area of the probe), and v_{sh} is the speed at which ions are accelerated to at the sheath edge (assumed to be the Bohm velocity $\sqrt{T_e/M_i}$).

It is worth pointing out that, as shown in Sec. IV, significant ion drift velocities have been found. Additionally, LIF measurements of the IVDF in similar operating conditions [31] showed that the IVDF was anisotropic along the centerline. For the electrons, significant drift velocities ($M_e > 1$, where M_e is the electron Mach number) were estimated along the centerline in Ref. [32]. These observations indicate that corrections for density and electron temperature are needed. However, this would require a self-consistent treatment of the potential structure relative to the probe surface as a function of the angle of the surface normal relative to the flow, and also would need to account for the anisotropy of ion drift and the IVDF. Such a treatment is outside the scope of this work, but it should be noted that these effects might result in an overestimation of density and electron temperature (and therefore wave energy).

IV. Results

To evaluate the energy transferred to ions by IAT it is necessary to decouple this mechanism from others that might also add energy to the ions. Based on wave energy spectra taken in hollow cathode plumes operating at high current-to-flow rate ratios the dominant mode appears to be one that has most of its energy content in the <100 kHz frequency range. This is generally associated with ionization instability fluctuations that can reach large amplitudes [6]. To isolate the effects of IAT, experiments were conducted at discharge currents of ≥70 A. Ion heating as a function of discharge current and cathode flow rate were parametrically evaluated for five operating conditions, shown in Table 1. (Note that the standard used for flow rate is 25°C and 760 torr). IV curves for the three flow rates are shown in Fig. 4. Voltage and currents shown are accurate to within 1 V and 1 A, respectively. To match the plasma conditions previously performed on this cathode design at JPL [13] (because the plasma properties were extensively measured), background pressure was controlled to 2.2×10^{-4} torr by flowing xenon through a leak valve.

A. Steady-State Langmuir Probe Measurements

Plasma density, shown in Fig. 5, was determined using Eq. (9). Uncertainties are not presented because the dominant uncertainty, caused by the high particle drifts and discussed in Sec. II, is beyond the scope of this work to estimate. A first-order calculation indicates these calculations to be within a factor of 2.

Electron temperature, which is needed to determine IAT wave energy per Eqs. (4) and (8), is shown in Fig. 6. Values of 2–3 eV were found, consistent with values reported by Jorns et al. [9]. The measurements for the 70 A case at $z = 18$ and 20 mm locations are absent due to data integrity concerns. An uncertainty analysis based solely on curve fitting shows an uncertainty <1%, with the following caveats: data were only fitted on a small region along the lower portion of the exponential, a linear fit was used for subtraction of the ion saturation current, and no flow effects were considered. As with density, particle drift effects are thought to be the dominant source of uncertainty.

B. RPA Measurements

The ion energy distribution function measurements obtained with the RPA in the far plume on-axis are shown in Fig. 7. The change from 70 to 100 A at 10 sccm produced no appreciable change to the IEDF, but increasing current to 130 A resulted in an increase in maximum energy by ∼10 eV, with the most probable energy relatively unchanged. Note that the hump in the 130 A, 10 sccm signal around 60 eV is believed to be due to the numerical differentiation performed on raw data with low signal-to-noise ratio. All cases showed maximum energies greater than the ∼20 V discharge voltage. The effect of increasing flow rate at 130 A was more apparent, having the opposite effect to increasing current: the mean energy decreases as does the maximum. This follows the trends of Ref. [9] that showed dampening of IAT by ion-neutral collisions, reducing ion heating.

Table 1 Operating conditions

Discharge current [A]	Discharge voltage [V]	Flow rate [Std. cm^3/s]
70	15.4	10
100	17.4	10
130	21.0	10
130	18.2	15
130	16.8	20

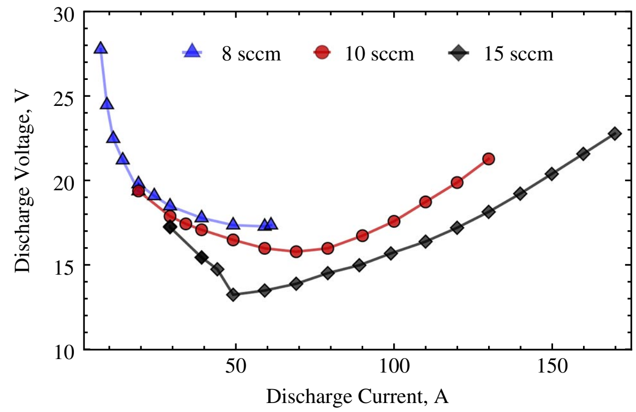

Fig. 4 Discharge voltage verus discharge current for various flow rates.

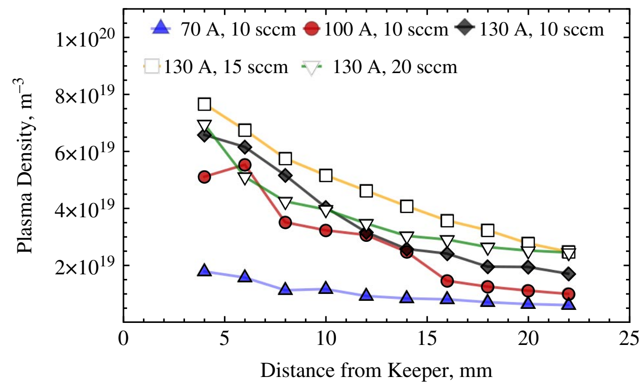

Fig. 5 Plasma density based on ion saturation current measurements from a cylindrical Langmuir probe.

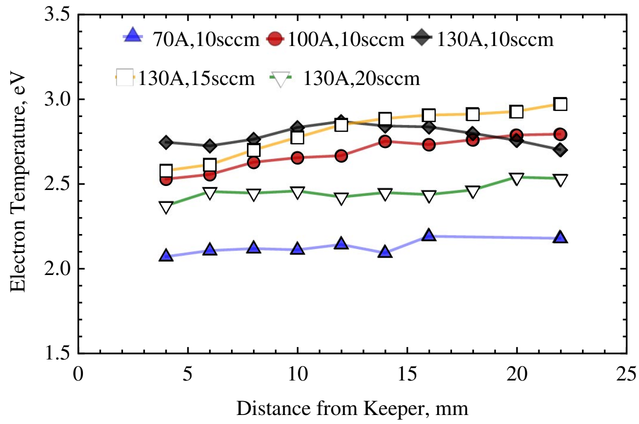

Fig. 6 Electron temperature versus distance downstream of the cathode keeper face.

C. LIF Measurements

An example of the signal obtained from LIF is shown in Fig. 8 for the 70 A, 10 sccm operating condition at three locations in the plume. At the keeper orifice ($z = 0$ mm) it can be approximated by a single

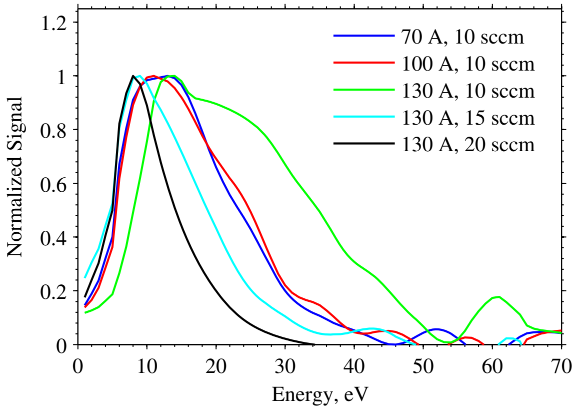

Fig. 7 Axial ion energy distribution measurements taken by RPA at 0.35 m downstream of the cathode keeper face. The curves are normalized to maximum signal.

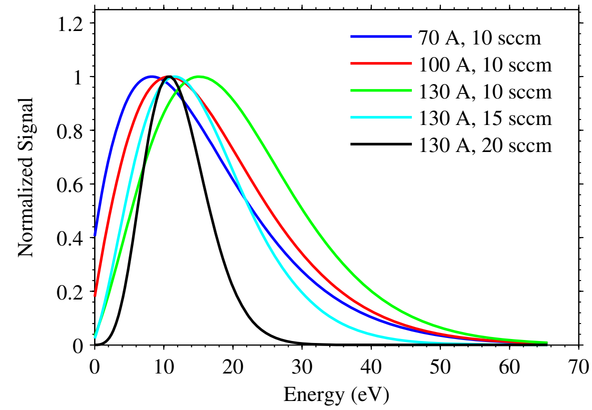

Fig. 9 Centerline IEDFs at location of peak ion temperature versus distance downstream of keeper face using a Gaussian fit to the drifting population. The curves are normalized to maximum signal.

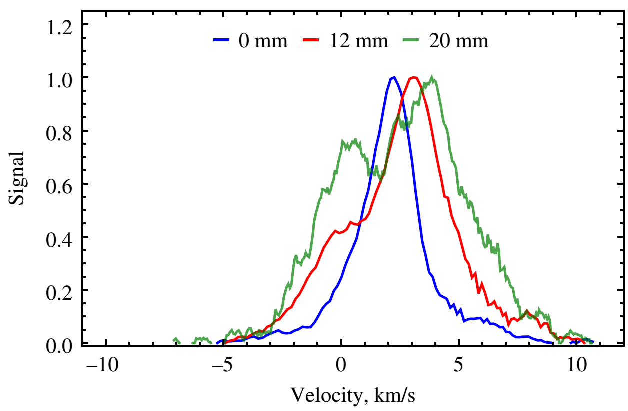

Fig. 8 Centerline IVDFs for the 70 A, 10 sccm operating condition at various locations downstream. Each plot is normalized by the maximum intensity and filtered using a 9-point moving average.

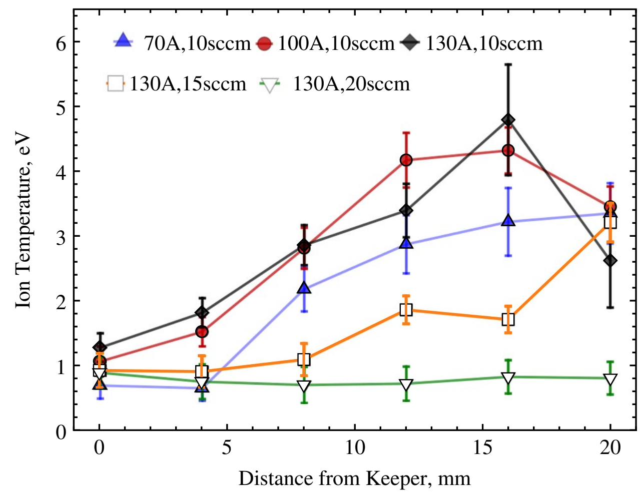

Fig. 10 Ion temperature versus distance downstream of the cathode keeper face for the drifting population, as measured by LIF.

Gaussian curve fit and corresponds to an ion temperature of ~1 eV. This is consistent with classical heating mechanisms inside the cathode, presumed to be caused by a cascade of ions falling through wall sheath potentials, undergoing charge-exchange collisions, and being resistively heated as shown by the modeling by [20]. Downstream the distribution broadens to nonclassical values, and a second peak forms nearly centered at 0 km/s. One possible explanation for this population is ionization, for which the mean free path is 2–3 cm based in this plasma. Charge-exchange could also contribute to this population because the mean free path is of the same order as that for ionization in this region, estimated using the simplified neutral gas model in Sec. V. Another observation is the lack of a tail on the distribution typically associated with resonant wave-particle interactions [13,33]. Although reasons for the absence are not understood at this time, it is possibly due to a relatively small number of particles able to interact with the wave, or that thermalization of that interaction takes place rapidly due to ion-ion or ion-neutral collisions due to the high density of the near plume. Investigations into the source of the slow population, its effect on IAT, and the possible thermalization effects of wave-particle interactions for this plasma are ongoing.

To enable comparison to the far-field IEDF results obtained by the RPA in Fig. 7, IEDFs calculated from LIF measurements are shown in Fig. 9 at the $z = 12$ mm, for the fast population only. Although not reported here, for $z \geq 20$ mm, the maximum ion velocity remains nearly constant, and so these LIF-derived IEDFs are representative of that which is expected to exist at the RPA location. These results follow the same qualitative trends in relation to mass flow and discharge current as the axial RPA results, with maximum ion energies also similar.

The results for ion temperature are shown in Fig. 10. We observe that ion heating is weakly dependent on current but strongly dependent on flow rate. However, all cases at 10 sccm show increasing temperature with distance downstream. For the case of increasing flow rate the ion heating rate is suppressed and nearly flat for the 20 sccm case. The most probable ion velocities are shown in Fig. 11. All cases show a gradual increase in drift velocity with

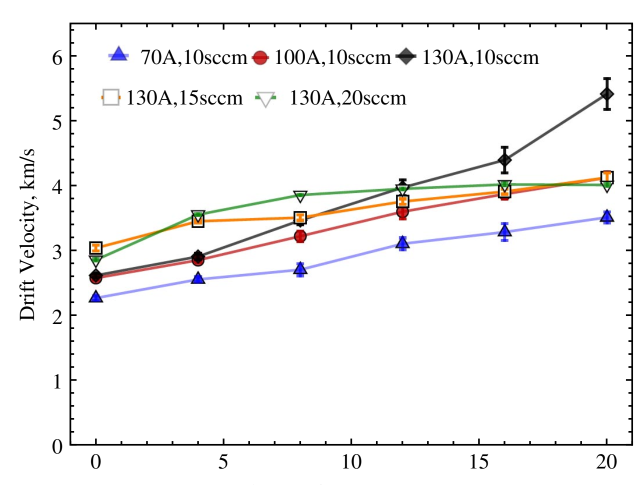

Fig. 11 Drift velocity versus distance downstream of the cathode keeper face for the drifting population, as measured by LIF.

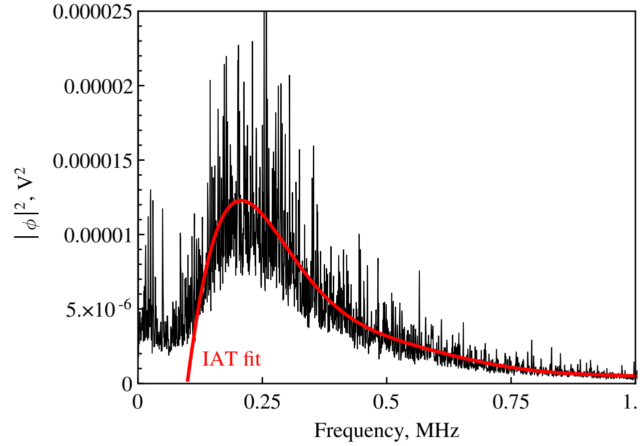

Fig. 12 Example of raw plasma potential amplitude spectrum for the 130 A, 10 sccm, operating condition at $z = 16$ mm.

distance from the keeper face. The mechanism responsible for the acceleration could possibly be due to pressure or potential gradients, but is not fully understood at this time.

D. Wave Energy Measurements

To isolate the wave energy associated with the IAT mode from the low-frequency fluctuations, typically at frequencies <100 kHz, the raw spectrum of signal power (i.e., $|\tilde{\phi}|^2$) was fit to a polynomial forced to terminate to zero amplitude at approximately 100 kHz. This ad hoc approach was used because the spectral profile of the low-frequency fluctuations is not known, and because the majority of conditions resulted in an IAT-dominant spectrum. Therefore this approach to spectral curve-fitting should introduce little uncertainty to the integrated spectral power. An example of a fluctuation spectrum and the curve fit used to determine the total IAT spectral power is shown in Fig. 12. The IAT power is clearly defined, and the fluctuations below ~100 kHz are ignored. This plot illustrates the inverse cascade of wave energy from high to low frequencies, which is consistent with a turbulent spectrum (cf. Ref. [34] Chap. 1). The wave energy values were not reported for cases where it was not possible to distinguish between the two modes. Figure 13 shows contour plots of the spectral power evolution with distance into the plume, illustrating increase in power at higher frequencies followed by a reduction toward low frequencies near the anode.

Using Eq. (4) and these integrated spectral powers, the wave energy density was calculated and is shown below in Fig. 14. Note that the wave energies for the 70 A, 10 sccm condition are not reported for $z > 14$ mm due to the inability to isolate the IAT component. The first general trend found is that increasing gas flow rate correlated with decreasing wave energy, possibly due to larger damping of the IAT mode by ion-neutral collisions. The second trend is that increasing discharge current correlated with increasing wave energy. However, the peak wave energy for the 100 A, 10 sccm case was higher than the 130 A, 10 sccm case, which differs from the trend seen in Ref. [9] (for similar currents but at 15 sccm instead of 10 sccm), which showed a monotonic increase in total wave energy with discharge current. The correlation of wave energy with discharge current is not obvious because the growth term depends not only on current but also on the relative electron drift velocity and particle temperatures, as well as on the specific nonlinear saturation mechanisms of the turbulent energy spectrum. This nonmonotonic increase of IAT with discharge current remains an open issue.

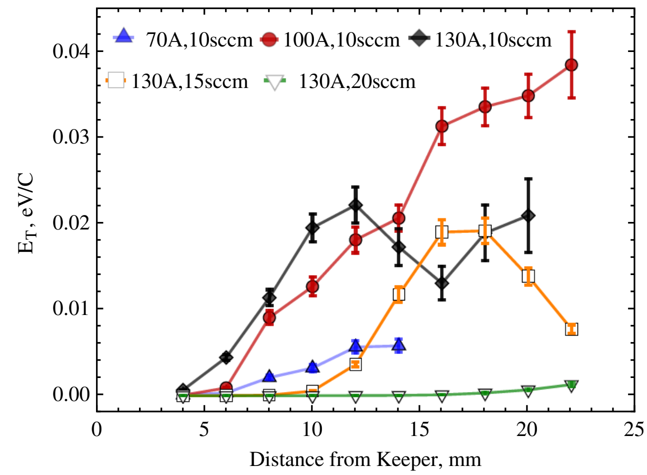

Fig. 14 Wave energy versus distance downstream of the cathode keeper face.

V. Discussion

As discussed in the Introduction, there is evidence for a correlation between ion energy in the far plume and wave energy associated with IAT wave energy. Indeed, the results of this study (as shown in Figs. 10 and 14) show similar qualitative trends in both ion temperature and wave energy as discharge current and flow rate are varied, resembling correlations first noted in Ref. [13]. These observations also make intuitive sense in that the waves are primarily

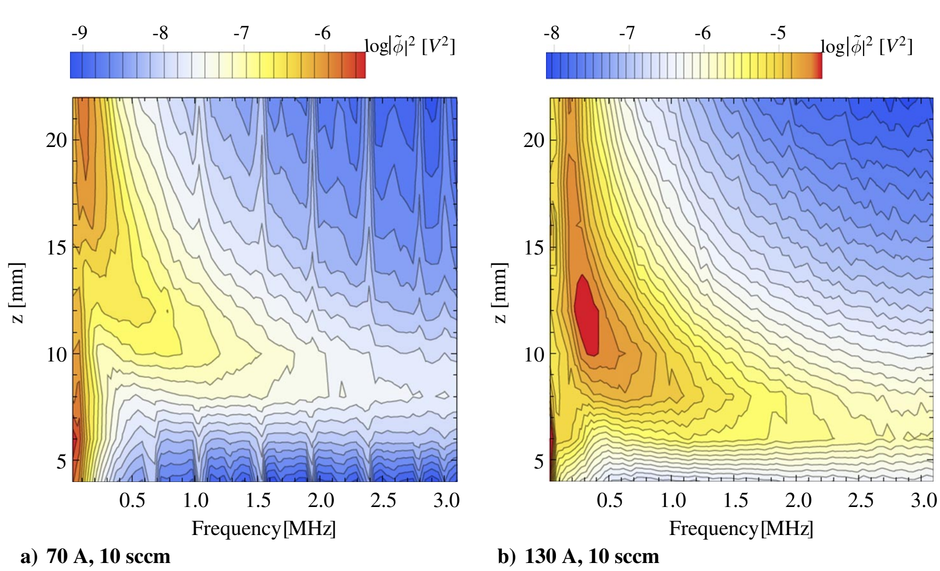

Fig. 13 Wave fluctuation power spectrum evolution with distance downstream for two different operating conditions. (Note that the intensity scales are different for the two operating conditions.)

carried by ion motion and therefore an increase in wave energy should lead to an effective increase in ion temperature. It should be noted that we cannot rule out other mechanisms that could also contribute to ion heating. For example, it is possible that there could be a potential drop along the centerline that could accelerate ions. Although plasma potential was not measured in this experiment, no measurements in the literature indicate potential drops sufficient to explain the high energies measured here by LIF and RPA diagnostics. Additionally, ions may gain energy from the low-frequency fluctuations. Because such a coupling has not been investigated, it is not possible to estimate this effect, and so we focus here exclusively on the effects of the IAT mode.

We will now explore this scaling quantitatively in the near plume, which could be useful for informing cathode simulations such as that in Ref. [20] that are attempting to self-consistently determine the wave energy density and ion temperature. The theoretical basis for that simulation is described in Ref. [14], which found the following scaling:

$$\Gamma_{\text{theory}} \approx \frac{\alpha\omega_{\text{pi}}}{\omega_0}\left(\frac{2}{\pi}\right)^{1/2} \tag{10}$$

where ω_{pi} is the ion plasma frequency, α is a constant of $\sim\mathcal{O}[10^{-2}]$, and ω_0 is the low-frequency cutoff related to the damping of acoustic modes at long length scales by processes such as geometric constraints or ion collisions. Here we briefly discuss simple models to estimate this cutoff frequency to enable a calculation of the scaling parameter based on Eq. (10) using background plasma measurements as inputs.

A. Low-Frequency Cutoff

The low-frequency damping due to geometric constraints comes from the eikonal/WKB approximation (cf. Ref. [35] Chap. 1) that states that the length scale of the plasma properties must be short relative to the wavelength in order for the mode to propagate. We approximate the length scale based on the density gradient: $L = n_0/\nabla n_0 = 2\pi/k_c$, where k_c is the cutoff wavenumber. Substituting k_c into Eq. (1) gives the low frequency cutoff as:

$$\nu_{c,L} = 2\pi\frac{(c_s + V_{\text{di}})}{L} \tag{11}$$

Another relevant parameter for the low frequency cutoff is the ion-neutral collision frequency, $\nu_{c,\text{in}}$. For this weakly ionized plasma we assume that the dominant collisions are due to charge-exchange and elastic ion-neutral collisions, the frequency of which is determined by the following:

$$\nu_{c,\text{in}} = \nu_{\text{CEX}} + \nu_{\text{el}} = n_n v_i(\sigma_{\text{CEX}} + \sigma_{\text{el}}) \tag{12}$$

where n_n is the neutral gas density, $v_i = \sqrt{T_i/m_i}$ is the ion thermal velocity, and the cross sections for charge-exchange and elastic collisions are, using Ref. [36], approximated by $\sigma_{\text{CEX}} = (-0.8821 \ln|v_i - v_n| + 15.1262) \times 10^{-20}\ \text{m}^2$ and $\sigma_{\text{el}} = 6.42 \times 10^{-16}/|v_i - v_n|\ \text{m}^{-2}$, respectively. To approximate the neutral gas density, collisions were neglected and it was assumed to expand with a divergence half-angle of $\theta = 22.5^{\circ}$ [37]. Ionization was estimated to have a relatively small effect on neutral gas density for this plume divergence plasma density, and so was neglected. This results in $n_n = Q_n/v_{n0}\pi(r_0 + \theta z)^2$, where Q_n is the neutral particle flow rate, v_{n0} is the neutral gas thermal velocity (approximated as $\sqrt{T_n/m_n}$ and assuming T_n, the neutral gas temperature is $\approx$1000 K), and r_0 is the keeper orifice radius. The results for these low cutoff frequency calculations show that ω_0 ranges from 50 to 700 kHz using the using the neutral collision frequency, and from 5 to 120 kHz using the density gradient length scale. The higher cutoff frequency of the two calculated is most physically relevant, and for the tested conditions the low-frequency cutoff was dominated by the ion neutral collision frequency.

B. Scaling Parameter

The experimentally determined scaling parameter is $\Gamma_{\text{Meas}} = \Delta T_i/\Delta E_T$, where ΔT_i and ΔE_T are the changes in ion temperature and wave energy density relative to the conditions at the keeper face (approximated by measurements at $z = 4$ mm). Figure 15a shows both Γ_{Meas} (where ΔT_i at the location of the E_T measurements was estimated by interpolation of the LIF-obtained T_i) and Γ_{Theory} calculated using Eq. (10) on a semilog scale. Because of the large number of assumptions, no uncertainty analysis for the theoretical estimate was performed. Figure 15b shows the scaling parameters accounting for propagation of uncertainty on a linear scale. Upstream of $z = 12$ mm the uncertainties in Γ_{Meas} are large due to the large relative uncertainties and small changes in parameters before the exponential rise downstream. For this reason we focus on the region $z \geq 12$ mm, where the scaling parameters converge toward the theoretical estimates. Additionally, because no appreciable changes in either ion temperature or wave energy were observed for the 130 A, 20 sccm operating condition, scaling parameters for those measurements are omitted from both figures. These figures show that Γ_{Meas} is very large in the region nearest the keeper and decreases exponentially downstream, almost monotonically. Some potential explanations for the deviation between Γ_{Meas} and Γ_{Theory} are proposed here.

The first uncertainty considered is the value of ion temperature. As discussed, the degree of saturation broadening cannot be fully determined without repeating the experiment due to uncertainties in validity of the two-level energy model for this transition. Additionally, it is possible that one or both of the ion distributions being fitted are not Gaussian. However, in the near-keeper region the

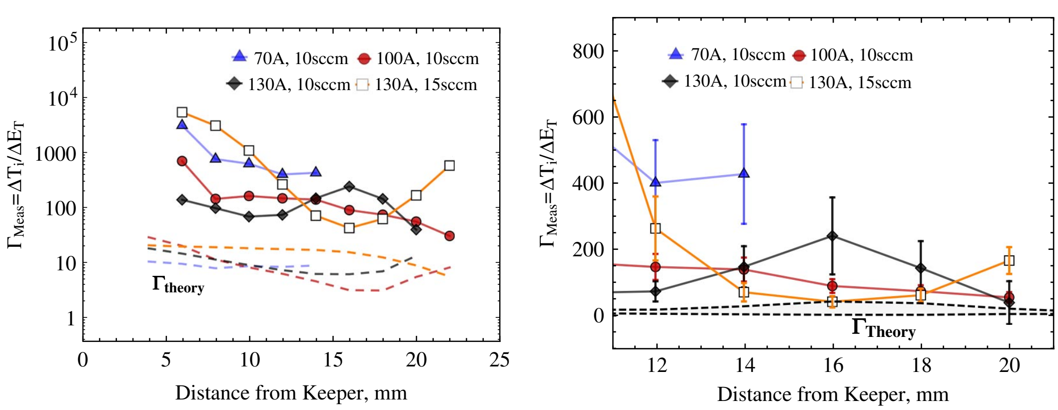

a) Measured (solid) and theoretical scaling parameter (dashed)

b) Measured scaling parameters with uncertainties for z > 10 mm. Only the bounds of the theoretical scaling parameter are shown for clarity

Fig. 15 Scaling parameters.

temperature estimates would have to be off by 2–3 orders of magnitude to explain the disagreement in Γ. The wave energy measurements could also have been affected due to the inevitable perturbation of the plasma because the probe was large in relation to the plume diameter near the keeper. Although not quantitatively characterized in this work, there was a clear effect of the probe on the global behavior of the cathode discharge when the probe was at the 4 mm downstream location, reducing the discharge voltage by as much as 10%. The effect on discharge current decreased for locations farther downstream.

Another possible explanation for these observations could be that the fluid formulation used to derive the scaling parameter in Eq. (10) in Ref. [14] is not valid in the region nearest the keeper, but becomes increasingly valid with distance downstream where the instability saturates. The theory assumes slowly varying plasma parameters with respect to the wave growth rate, which may not be the case in regions nearest the keeper. Also, the α parameter from Eq. (10) may not be constant in the plume. Near the anode, where the IAT is more fully developed, there is agreement to theory within a factor of 10 for two operating conditions, which is encouraging and may indicate that the theory can be improved to better account for regions corresponding to the initial growth of the instability.

VI. Conclusions

In this study, measurements of the correlation between ion acoustic turbulence (IAT) wave energy and ion heating for hollow cathodes used for electric propulsion were obtained for the first time. Although there is a clear qualitative correlation between the two parameters, they are not 1:1, which suggests that there must be a scaling parameter. The results were examined in the context of previous quasilinear attempts to derive this parameter. One of these theories, which has been successfully applied in a self-consistent model, suggests that the scaling parameter should depend uniquely on background plasma parameters and a so-called low cutoff frequency. This calculated parameter has been used in combination with two models for the cutoff frequency and found agreement to within an order of magnitude, in the region of the plume where IAT was fully developed, for two operating conditions. This suggests that this may be a promising analytical hierarchy to relate IAT to ion temperature. However, the scaling parameter was measured to be much higher than predicted near the cathode keeper. These disagreements with theory could be due to experimental uncertainties or assumptions in the analytical theory that neglect rapid variations in plasma parameters that may occur in the region of the plume where IAT is developing.

It is important to understand ion temperature in hollow cathode plumes because of the potential damage caused by energetic ions, and more generally because it offers insight into the energy balance of IAT that affects the overall macroscopic properties in the plume. Although the current study focused on ion heating along the centerline only, it will provide a database for theory evaluation that may lead to application in regions off-axis. In particular, there is interest in simulating the ion conditions along the keeper face to better understand keeper erosion, which is the focus of ongoing work. The results from this research are currently being used to validate models being developed for the first time that self-consistently model hollow cathode plumes, which predict ion temperatures within a factor of two [20] compared with these results. That model will enable predictions of cathode lifetime, aid cathode design, and inform the selection of operating conditions to mitigate erosion caused from energetic ion production.

Acknowledgments

The research described in this paper was carried out at the Jet Propulsion Laboratory, California Institute of Technology, under a contract with the National Aeronautics and Space Administration. It was also supported by the National Science Foundation Graduate Research Fellowship under Grant No. DGE-1144087. Part of this work has been supported by Spain's R&D National Plan, grant number ESP2013-41052-P. The support of the joint NASA GRC and JPL development of HERMeS by NASA's Space Technology Mission Directorate through the Solar Electric Propulsion Technology Demonstration Mission (SEP TDM) project is gratefully acknowledged. The authors would also like to acknowledge Ray Swindlehurst and Nowell Niblitt for their assistance in running the experimental facility, and Taylor Matlock for assistance in interpreting Langmuir probe measurements.

References

[1] Polk, J., "An Overview of the Nuclear Electric Xenon Ion System (NEXIS) Program," *39th AIAA/ASME/SAE/ASEE Joint Propulsion Conference & Exhibit*, AIAA Paper 2003-4713, July 2003. doi:10.2514/6.2003-4713

[2] Kamhawi, H., Huang, W., Haag, T., Yim, J., Chang, L., Clayman, L., Herman, D., Shastry, R., Thomas, R., Griffith, C., Myers, J., Williams, G., Mikellides, I. G., Hofer, R., Polk, J. E., and Goebel, D. M., "Overview of the Development of the Solar Electric Propulsion Technology Demonstration Mission 12.5 kW Hall Thruster," *50th AIAA/ASME/SAE/ASEE Joint Propulsion Conference & Exhibit*, AIAA Paper 2014-3898, July 2014. doi:10.2514/6.2014-3898

[3] Rawlin, V. K., "Internal Erosion Rates of a 10-kW Xenon Ion Thruster," *24th AIAA/ASME/SAE/ASEE Joint Propulsion Conference*, AIAA Paper 1988-2912, July 1988.

[4] Brophy, J. R., and Garner, C. E., "Tests of High Current Hollow Cathodes for Ion Engines," *AIAA/ASME/SAE/ASEE 24th Joint Propulsion Conference*, AIAA Paper 1988-2913, Aug 1988. doi:10.2514/6.1988-2913

[5] Friedly, V., and Wilbur, P., "High Current Hollow Cathode Phenomena," *Journal of Propulsion and Power*, Vol. 8, No. 3, 1990, pp. 635–643. doi:10.2514/3.23526

[6] Goebel, D. M., Jameson, K. K., Katz, I., and Mikellides, I. G., "Potential Fluctuations and Energetic Ion Production in Hollow Cathode Discharges," *Physics of Plasmas*, Vol. 14, No. 10, 2007, Paper 103508. doi:10.1063/1.2784460

[7] Farnell, C. C., and Williams, J. D., "Measurement of Ion Energy Distributions Produced within an NSTAR Discharge Chamber," *40th Joint Propulsion Conference*, AIAA Paper 2004-3432, July 2004. doi:10.2514/6.2004-3432

[8] Chu, E., Goebel, D. M., and Wirz, R. E., "Reduction of Energetic Ion Production in Hollow Cathodes by External Gas Injection," *Journal of Propulsion and Power*, Vol. 29, No. 5, 2013, pp. 1155–1163. doi:10.2514/1.B34799

[9] Jorns, B. A., Mikellides, I. G., Goebel, D. M., and Ortega, A. L., "Mitigation of Energetic Ions and Keeper Erosion in a High-Current Hollow Cathode," *International Electric Propulsion Conference*, IEPC Paper 2015-134, July 2015.

[10] Mikellides, I. G., Katz, I., Goebel, D. M., and Jameson, K. K., "Evidence of Nonclassical Plasma Transport in Hollow Cathodes for Electric Propulsion," *Journal of Applied Physics*, Vol. 101, No. 6, 2007, Paper 063301. doi:10.1063/1.2710763

[11] Jorns, B. A., Mikellides, I. G., and Goebel, D. M., "Temporal Fluctuations in a 100-A LaB6 Hollow Cathode," *33rd International Electric Propulsion Conference*, IEPC Paper 2013-385, Oct. 2013.

[12] Jorns, B. A., Mikellides, I. G., and Goebel, D. M., "Ion Acoustic Turbulence in a 100-A LaB6 Hollow Cathode," *Physical Review E*, Vol. 90, No. 6, 2014, Paper 063106. doi:10.1103/PhysRevE.90.063106

[13] Jorns, B., Goebel, D. M., and Mikellides, I. G., "Investigation of Energetic Ions in a 100-A Hollow Cathode," *50th AIAA/ASME/SAE/ASEE Joint Propulsion Conference*, AIAA Paper 2014-3826, July 2014. doi:10.2514/6.2014-3826

[14] Jorns, B. A., Lopez-Ortega, A., and Mikellides, I. G., "First-Principles Modeling of IAT-Driven Anomalous Resistivity in Hollow Cathodes Discharges I: Theory," *52nd AIAA/SAE/ASEE Joint Propulsion Conference*, AIAA Paper 2016-4626, July 2016. doi:10.2514/6.2016-4626

[15] Ho, A. K., Jorns, B. A., Goebel, D. M., Mikellides, I. G., and Lopez-Ortega, A., "Wear Test Demonstration of a Technique to Mitigate Keeper Erosion in a High-Current LaB6 Hollow Cathode," *52nd AIAA/SAE/ASEE Joint Propulsion Conference*, AIAA Paper 2016-4836, July 2016. doi:10.2514/6.2016-4836

[16] Williams, G., Smith, T., Domonkos, M., Gallimore, A., and Drake, R., "Laser-induced Fluorescence Characterization of Ions Emitted from Hollow Cathodes," *IEEE Transactions on Plasma Science*, Vol. 28,

No. 5, 2000, pp. 1664–1675.
doi:10.1109/27.901252

[17] Georgin, M., Durot, C., and Gallimore, A. D., "Preliminary Measurements of Time Resolved Ion Velocity Distributions Near a Hollow Cathode," *International Electric Propulsion Conference*, IEPC Paper 2015-106, July 2015.

[18] Kadomtsev, B. B., *Plasma Turbulence*, 1st ed., Academic Press, New York, 1965, Chap. 4.

[19] Stix, T., *Waves in Plasmas*, 1st ed., AIP-Press, New York, 1992.

[20] Lopez-Ortega, A., Mikellides, I. G., and Jorns, B. A., "First-Principles Modeling of IAT-Driven Anomalous Resistivity in Hollow Cathode Discharges II: Numerical Simulations and Comparisons with Experiments," *52nd AIAA/SAE/ASEE Joint Propulsion Conference*, AIAA Paper 2016-4627, July 2016.
doi:10.2514/6.2016-4627

[21] Manzella, D. H., "Stationary Plasma Thruster Ion Velocity Distribution," AIAA Paper 1994-3141, Aug. 1994.

[22] Hargus, W. A., and Charles, C. S., "Near Exit Plane Velocity Field of a 200-Watt Hall Thruster," *Journal of Propulsion and Power*, Vol. 24, No. 1, 2008, pp. 127–133.
doi:10.2514/1.29949

[23] Huang, W., Smith, T. B., and Gallimore, A. D., "Obtaining Velocity Distribution Using a Xenon Ion Line with Unknown Hyperfine Constants," *40th AIAA Plasmadynamics and Laser Conference*, AIAA Paper 2009-4226, June 2009.

[24] Pawelec, E., Mazouffre, S., and Sadeghi, N., "Hyperfine Structure of Some Near-Infrared XeI and XeII Lines," *Spectrochimica Acta-Part B*, Vol. 66, No. 6, 2011, pp. 470–475.
doi:10.1016/j.sab.2011.05.009

[25] Manola, S., and Konjevic, N., "Stark Broadening of the Singly Ionized Xenon Line: Temperature Variation," *Physical Review A*, Vol. 38, No. 11, 1988, pp. 5742–5744.
doi:10.1103/PhysRevA.38.5742

[26] Huang, W., "Study of Hall Thruster Discharge Channel Wall Erosion via Optical Diagnostics by Wensheng Huang," Ph.D. Dissertation, Department of Aerospace Engineering, Univ. of Michigan, 2011.

[27] Chaplin, V. H., Conversano, R. W., Lobbia, R. B., Ortega, A. L., Mikellides, I. G., and Hofer, R. R., "Laser-Induced Fluorescence Measurements of the Acceleration Zone in the 12.5 kW HERMeS Hall Thruster," *International Electric Propulsion Conference*, IEPC Paper 2017-229, Oct. 2017.

[28] Smith, T. B., "Deconvolution of Ion Velocity Distributions from Laser-Induced Fluorescence Spectra of Xenon Electrostatic Thruster Plumes," Ph.D. Dissertation, Dept. of Aerospace Engineering, Univ. of Michigan, 2003.

[29] Hutchinson, I., *Principles of Plasma Diagnostics*, 2nd ed., Cambridge Univ. Press, Cambridge, U.K., 2005.

[30] Chen, F. F., "Langmuir Probe Diagnostics," *Mini-Course on Plasma Diagnostics, IEEE-ICOPS Meeting*, June 2003.

[31] Dodson, C. A., Jorns, B. A., and Wirz, R. E., "Ion Acoustic Wave Propagation and Heating in a High-Current Hollow Cathode Plume," *International Electric Propulsion Conference*, IEPC Paper 2017-398, Oct. 2017.

[32] Jorns, B. A., Dodson, C. A., Goebel, D. M., and Wirz, R. E., "Propagation of Ion Acoustic Wave Energy in the Plume of a High-Current LaB6 Hollow Cathode," *Physical Review E*, Vol. 96, No. 2, 2017, Paper 023208.
doi:10.1103/PhysRevE.96.023208

[33] Ishihara, O., and Hirose, A., "Quasilinear Mechanism of High-Energy Ion-Tail Formation in the Ion-Acoustic Instability," *Physical Review Letters*, Vol. 46, No. 12, 1981, pp. 771–774.
doi:10.1103/PhysRevLett.46.771

[34] Tsytovich, V., *Theory of Turbulent Plasma*, Plenum Publishing Corporation, New York, 1977.

[35] Swanson, D., *Plasma Waves*, IOP Publ. Ltd., New York, 2003.

[36] Levko, D., Krasik, Y. E., Vekselman, V., and Haber, I., "Two-Dimensional Model of Orificed Micro-Hollow Cathode Discharge for Space Application," *Physics of Plasmas*, Vol. 20, No. 8, 2013, Paper 083512.
doi:10.1063/1.4818969

[37] Katz, I., Mikellides, I., and Goebel, D., "Model of the Plasma Potential Distribution in the Plume of a Hollow Cathode," *40th Joint Propulsion Conference*, AIAA Paper 2004-4108, July 2004.
doi:10.2514/6.2004-4108

L. B. King
Associate Editor